the FEBS Journal

Aromatic stacking interactions govern catalysis in aryl-alcohol oxidase

Patricia Ferreira[1], Aitor Hernández-Ortega[2,†], Fátima Lucas[3], Juan Carro[2], Beatriz Herguedas[1,‡], Kenneth W. Borrelli[3], Victor Guallar[3,4], Angel T. Martínez[2] and Milagros Medina[1]

1 Departamento de Bioquímica y Biología Molecular y Celular, Facultad de Ciencias, Universidad de Zaragoza, and Instituto de Biocomputación y Física de Sistemas Complejos, Zaragoza, Spain
2 Centro de Investigaciones Biológicas, Consejo Superior de Investigaciones Científicas, Madrid, Spain
3 Joint Barcelona Supercomputing Center-Centre for Genomic Regulation-Institute for Research in Biomedicine Research Program in Computational Biology, Barcelona Supercomputing Center, Barcelona, Spain
4 Institució Catalana de Recerca i Estudis Avançats, Barcelona, Spain

Keywords
aromatic stacking; aryl-alcohol oxidase; catalytic mechanism; GMC oxidoreductases; steady-state and pre-steady state kinetics

Correspondence
P. Ferreira, Departamento de Bioquímica y Biología Molecular y Celular, Facultad de Ciencias, Universidad de Zaragoza, Pedro Cerbuna 12, 50009 Zaragoza, Spain
Fax: +34976762123
Tel.: +34876553774
E-mail: ferreira@unizar.es

Present addresses:
†Manchester Institute of Biotechnology, University of Manchester, Manchester, UK
‡Medical Research Council Laboratory of Molecular Biology, Cambridge, UK

(Received 29 October 2014, revised 10 January 2015, accepted 28 January 2015)

doi:10.1111/febs.13221

Aryl-alcohol oxidase (AAO, EC 1.1.3.7) generates H_2O_2 for lignin degradation at the expense of benzylic and other π system-containing primary alcohols, which are oxidized to the corresponding aldehydes. Ligand diffusion studies on *Pleurotus eryngii* AAO showed a T-shaped stacking interaction between the Tyr92 side chain and the alcohol substrate at the catalytically competent position for concerted hydride and proton transfers. Bi-substrate kinetics analysis revealed that reactions with 3-chloro- or 3-fluorobenzyl alcohols (halogen substituents) proceed via a ping–pong mechanism. However, mono- and dimethoxylated substituents (in 4-methoxybenzyl and 3,4-dimethoxybenzyl alcohols) altered the mechanism and a ternary complex was formed. Electron-withdrawing substituents resulted in lower quantum mechanics stacking energies between aldehyde and the tyrosine side chain, contributing to product release, in agreement with the ping–pong mechanism observed in 3-chloro- and 3-fluorobenzyl alcohol kinetics analysis. In contrast, the higher stacking energies when electron donor substituents are present result in reaction of O_2 with the flavin through a ternary complex, in agreement with the kinetics of methoxylated alcohols. The contribution of Tyr92 to the AAO reaction mechanism was investigated by calculation of stacking interaction energies and site-directed mutagenesis. Replacement of Tyr92 by phenylalanine does not alter the AAO kinetic constants (on 4-methoxybenzyl alcohol), most probably because the stacking interaction is still possible. However, introduction of a tryptophan residue at this position strongly reduced the affinity for the substrate (i.e. the pre-steady state K_d and steady-state K_m increase by 150-fold and 75-fold, respectively), and therefore the steady-state catalytic efficiency, suggesting that proper stacking is impossible with this bulky residue. The above results confirm the role of Tyr92 in substrate binding, thus governing the kinetic mechanism in AAO.

Abbreviations
AAO, aryl-alcohol oxidase; AAO_{red}, reduced AAO; CTC, charge transfer complex; GMC, glucose/methanol/choline oxidase (oxidoreductase superfamily); KIE, kinetic isotope effect; MM, molecular mechanics; QM, quantum mechanics.

Introduction

Aryl-alcohol oxidases (AAO, EC 1.1.3.7) are extracellular flavoproteins that typically catalyze the oxidative dehydrogenation of polyunsaturated alcohols using molecular oxygen as the final electron acceptor and producing hydrogen peroxide [1]. This activity was first reported in *Trametes versicolor* [2], and was later described in other white-rot basidiomycetes that are mainly responsible for lignin degradation in nature, such as *Pleurotus eryngii*, *Bjerkandera adusta* and *Phanerochaete chrysosporium* [3–7]. Lignin removal is a rate-limiting step for carbon recycling in land ecosystems, also playing a central role in paper pulp manufacture and the production of chemicals and biofuels from renewable lignocellulosic biomass [8]. The physiological role of AAO in wood-rotting basidiomycetes is to provide a continuous supply of extracellular H_2O_2, which is required as a substrate for ligninolytic peroxidases (in white-rot fungi) and as plant polysaccharides (in brown-rot fungi) [1,9].

AAO from *Pleurotus eryngii* has been intensively investigated [1,10–13]. This enzyme contains one molecule of non-covalently bound FAD that acts as a two-electron acceptor during oxidation of a wide range of benzylic and other aromatic and aliphatic polyunsaturated primary alcohols (reductive half-reaction). The oxidative half-reaction, whereby the FAD hydroquinone is oxidized by O_2, closes the catalytic cycle [12–14]. AAO also oxidizes some aromatic aldehydes via their hydrated (*gem*-diol) forms, suggesting similar mechanisms for alcohol and aldehyde oxidation [15].

The AAO crystal structure (PDB ID 3FIM) confirmed that it shares similar fold topology with other members of the glucose/methanol/choline oxidase (GMC) oxidoreductase superfamily [16], and a role in catalysis of two conserved active-site residues (His502 and His546 in *Pleurotus eryngii* AAO) was postulated [17]. Diffusion simulations of the reducing substrate towards the AAO active site, previously identified in the crystal structure, suggested an entrance channel next to the Gln395–Thr406 loop [18]. These studies additionally suggested that formation of the catalytically competent complex, requires significant displacements of side chains in the active-site environment (including Phe397), as well as the π–π stacking interaction with Tyr92 (Fig. 1) [18]. In contrast, the oxidative substrate migration did not require the above structural reorganization, even though Phe501 was shown to be essential for correct O_2 positioning [12].

A hydride transfer reaction assisted by a conserved active-site base is the consensus catalytic mechanism in the GMC superfamily [19–25]. An initial mechanistic

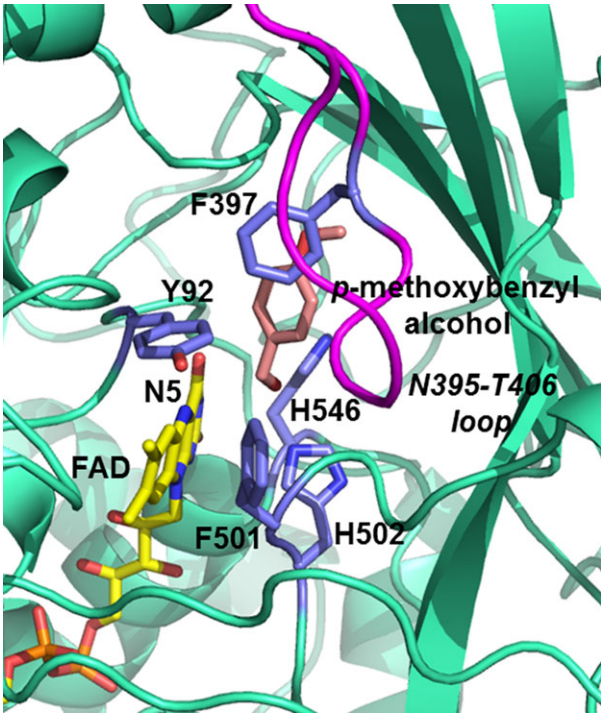

Fig. 1. Detail of the AAO active site with bound alcohol substrate. Position of 4-methoxybenzyl alcohol after migration simulations to the AAO active site using PELE software [50] (on the 3FIM crystal structure). The alcohol is located in the surroundings of two conserved histidines, three aromatic residues and the FAD isoalloxazine ring. Carbon atoms are shown in yellow, light pink and purple for the FAD, the alcohol and the rest of visible residues respectively. The Gln395–Thr406 loop is shown in magenta.

study on AAO, including analysis of substrate and solvent kinetic isotope effects (KIEs), suggested a concerted proton abstraction from the alcohol hydroxyl and hydride transfer from the alcohol α-carbon to FAD, without formation of a stable alkoxide intermediate [13]. Subsequent research combining site-directed mutagenesis and quantum mechanics/molecular mechanics (QM/MM) calculations confirmed the role of His502 as the AAO catalytic base [18]. Moreover, the combination of QM/MM profiles and solvent KIE data showed that the O–H bond cleavage for proton abstraction from the alcohol hydroxyl precedes the C_α–H bond cleavage for hydride transfer, although both processes are highly coupled. These observations revealed a non-synchronous concerted mechanism for alcohol oxidation by AAO [18]. This finding contrasts with the non-concerted mechanism previously reported for choline and methanol oxidases (EC 1.1.3.17 and EC 1.1.3.13, respectively), which includes a stable alkoxide intermediate, and provides an alternative mechanism for alcohol oxidation in the GMC superfamily

[26,27]. Subsequent studies indicated that hydride abstraction from the alcohol substrate by AAO is stereo-selective. Consequently, the interest in the study of the AAO reaction mechanism has expanded due to the enzyme's potential for de-racemization of chiral mixtures, as well as to the identification of new oxidative conversions, such as the recently described 5-hydroxymethyfurfural oxidation to 2,5-furandicarboxylic acid for production of renewable polyesters [28].

In the present study, various aromatic alcohol substrates (Fig. 2) have been used to complete the description of the AAO overall catalytic cycle and to evaluate the influence of the aromatic stacking interactions on catalysis. This latter aim was also addressed by using mutants at position Tyr92 to investigate its contribution to the AAO reaction mechanism. The results presented provide new insights into the catalytic mechanism of AAO, and, by extension, of the GMC superfamily.

Results

Influence of alcohol type on AAO kinetic mechanism: steady-state results

Double reciprocal plots of the initial rates of AAO reaction with various substituted benzyl alcohol substrates (Fig. 2) at various O_2 concentrations yielded two kinetic patterns. For 3,4-dimethoxybenzyl and 3-chloro-4-methoxybenzyl alcohols, the plots were linear and intersected to the left of the *y* axis (below zero with respect to the *x* axis) (Fig. 3A), as previously reported for 4-methoxybenzyl alcohol and 2,4-hexadien-1-ol [13]. This is indicative of a sequential reaction mechanism involving a ternary complex between AAO and its reducing/oxidizing substrates (Scheme 1, top loop). In contrast, a parallel line pattern was obtained for the two other substrates investigated, 3-chlorobenzyl and 3-fluorobenzyl alcohols (Fig. 3B), indicating a ping–pong mechanism (Scheme 1, bottom loop).

The steady-state kinetic parameters obtained by fitting the experimental data from the bi-substrate kinetics analysis to either Eqn (1) or Eqn (2) (describing

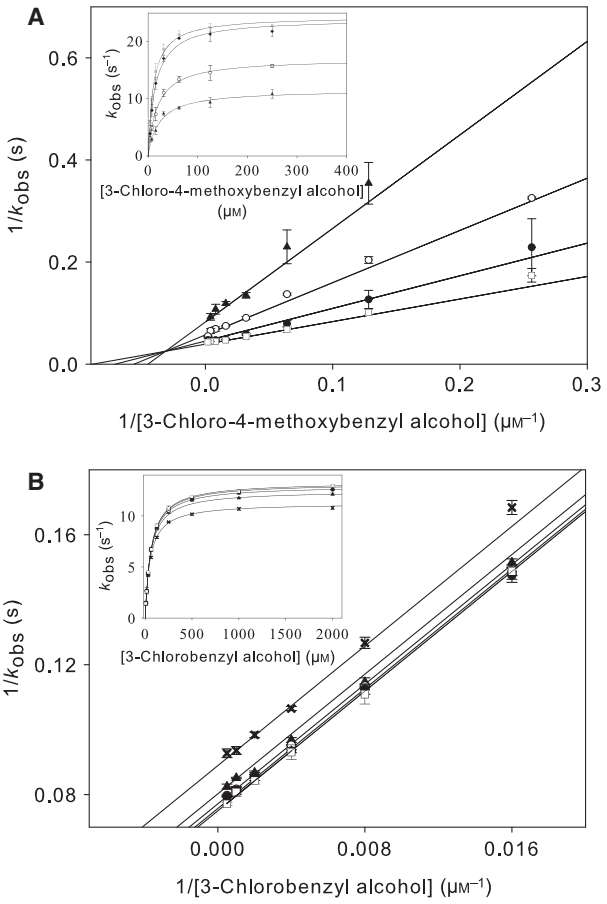

Fig. 3. Bi-substrate steady-state kinetics for AAO. Double reciprocal plot for the oxidation of 3-chloro-4-methoxybenzyl alcohol (A) and 3-chlorobenzyl alcohol (B) by native AAO, measured in 0.1 M phosphate buffer, pH 6, at 12 °C, as a function of the alcohol substrate concentration at fixed O_2 concentrations: 61 μM (crosses), 152 μM (black triangles), 319 μM (open circles), 668 μM (black circles) and 1520 μM (open squares). Direct plots are shown in the corresponding insets.

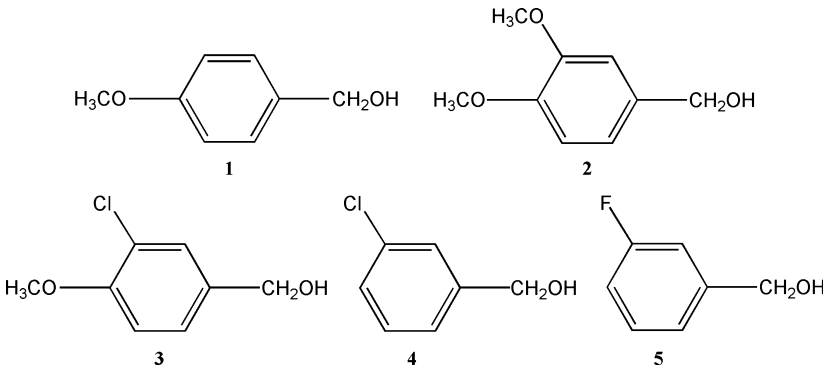

Fig. 2. Chemical structures of the alcohol substrates used in this study. (1) 4-methoxybenzyl alcohol, (2) 3,4-dimethoxybenzyl alcohol, (3) 3-chloro-4-methoxybenzyl alcohol, (4) 3-chlorobenzyl alcohol and (5) 3-fluorobenzyl alcohol.

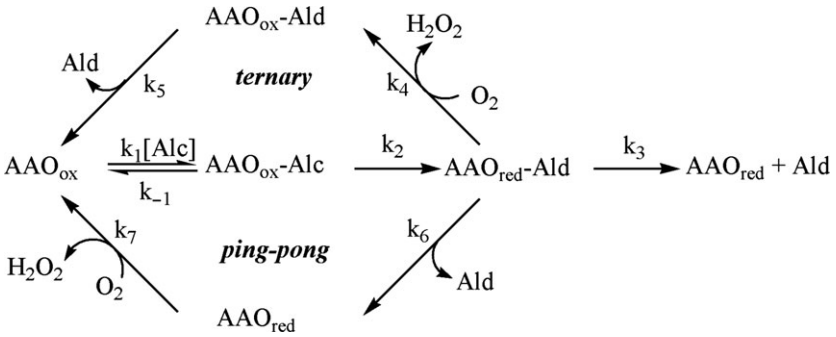

Scheme 1. Ternary and ping–pong mechanisms in AAO catalysis. The ternary and ping–pong mechanisms are described by the upper and lower loops, respectively, and the reaction on the right corresponds to aldehyde release in anaerobic experiments.

Table 1. Kinetic parameters for the steady-state reaction and for the pre-steady-state reductive half-reaction of AAO with five different alcohol substrates.

	Steady-state turnover					Reductive half-reaction	
Alcohol substrate	k_{cat} (s^{-1})	$K_{m(Al)}$ (μM)	$k_{cat}/K_{m(Al)}$ ($s^{-1}\cdot mM^{-1}$)	$K_{m(Ox)}$ (μM)	$k_{cat}/K_{m(Ox)}$ ($s^{-1}\cdot mM^{-1}$)	k_{red} (s^{-1})	K_d (μM)
4-Methoxybenzyl alcohol 1	129 ± 5	25 ± 3	5160 ± 650	348 ± 36	371 ± 41	115 ± 3	31 ± 2
3-Chloro-4-methoxybenzyl alcohol	29 ± 1	8 ± 1	3630 ± 470	214 ± 30	136 ± 20	95 ± 3	71 ± 10
3,4-Dimethoxybenzyl alcohol	57 ± 1	543 ± 39	105 ± 8	119 ± 11	479 ± 45	131 ± 10	838 ± 242
3-Chlorobenzyl alcohol	13 ± 1	62 ± 1	210 ± 4	10 ± 1	1300 ± 130	8 ± 1	58 ± 2
3-Fluorobenzyl alcohol	9 ± 1	164 ± 3	56 ± 1	7 ± 1	1400 ± 160	6 ± 1	180 ± 7

Measurements were performed in 0.1 M phosphate buffer, pH 6, at 12 °C. Steady-state kinetic constants were determined by varying the concentrations of both alcohol and O_2, and calculated by fitting to Eqn 1 (4-methoxybenzyl, 3-chloro-4-methoxybenzyl and 3,4-dimethoxybenzyl alcohols) or Eqn 2 (3-chlorobenzyl and 3-fluorobenzyl alcohols) describing either a ternary or ping-pong mechanism, respectively (see Materials and Methods). The pre-steady state observed reduction rate constants were fitted to Eqn 3. Means and standard deviations are provided. [1]Data from Ferreira *et al.* [13].

ternary or ping–pong mechanisms, respectively; see Experimental procedures), are summarized in Table 1. Turnover numbers (k_{cat}) calculated under substrate (alcohol and O_2) saturation conditions showed a similar dependence on the electronic nature of the substituents on the benzenic ring to those previously reported under air atmosphere [14]. The highest k_{cat} value (129 s^{-1} for 4-methoxybenzyl alcohol) and the lowest k_{cat} value (13 s^{-1} for 3-fluorobenzyl alcohol) were observed in the presence of electron donating and withdrawing substituents, respectively. However, the type of alcohol substrate also had a marked influence on $K_{m(O_2)}$, and therefore on the AAO affinity for O_2. Thus, the enzyme exhibits a considerably higher affinity for O_2 when the reaction takes place with alcohols that show a ping–pong mechanism in comparison with those forming a ternary complex: the $K_{m(O_2)}$ values for 3-chlorobenzyl and 3-fluorobenzyl alcohols are up to 35 times lower than that for 4-methoxybenzyl alcohol. As a consequence, the catalytic efficiency for O_2, $k_{cat}/K_{m(O_2)}$, is three times higher in the presence of alcohol substrates producing a ping–pong mechanism. Nevertheless, the catalytic efficiency with regard to the alcohol substrate, $k_{cat}/K_{m(Al)}$, is considerably decreased in the ping–pong mechanism due to both a reduction in k_{cat} and an increase in $K_{m(Al)}$ (Table 1).

AAO redox state during turnover and pre-steady-state kinetics: stopped-flow results

To investigate the rate-limiting step during oxidation of the various alcohols, we analyzed the redox state of the FAD cofactor during the steady-state turnover of AAO. To achieve this, equal volumes of the enzyme and of each alcohol at its saturating concentration were mixed in the stopped-flow equipment under air atmosphere (Fig. 4). The first spectra obtained after mixing showed slight displacement of flavin band I (462 nm), as well as a slight absorbance increase in the cases of 3-chloro-4-methoxybenzyl, 3-chlorobenzyl

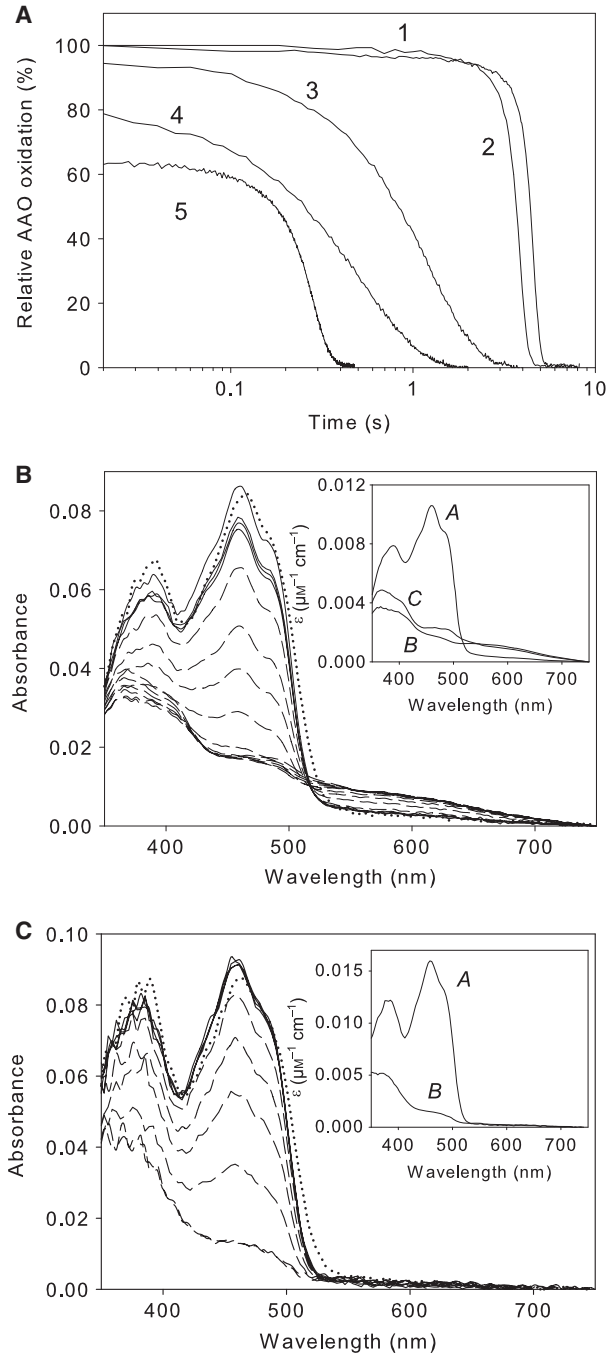

Fig. 4. AAO redox state during turnover with five alcohol substrates. Aerobic solutions of AAO (approximately 9 μM) were mixed in the stopped-flow spectrophotometer with equal volumes of saturating concentrations of the various alcohols in 0.1 M phosphate buffer, pH 6, at 25 °C and under aerobic conditions. (A) Time course of the reaction at 462 nm with: 2 mM 3-chlorobenzyl alcohol (trace 1), 5 mM 3-fluorobenzyl-alcohol (trace 2), 1 mM 3-chloro-4-methoxybenzyl alcohol (trace 3), 2 mM 4-methoxybenzyl alcohol (trace 4) and 4 mM 3,4-dimethoxybenzyl alcohol (trace 5). (B, C) AAO spectral changes upon mixing with 3-chloro-4-methoxybenzyl alcohol and 3-chlorobenzyl alcohol, respectively. The oxidized enzyme spectrum before mixing is shown as a dotted line. Spectra during the steady-state turnover phase (lag phase) are shown as solid lines at 0.003, 0.012, 0.026 and 0.051s in (A), and at 0.16, 0.33 and 0.98s in (B). Spectra after the steady-state turnover phase are shown as dashed lines at 0.24, 0.51, 0.71, 0.97, 1.5, 2.34, 8, 12, 18 and 27 s in (A), and at 3.6, 4.3, 4.59, 4.91, 10 and 60 s in (B). The corresponding insets show the spectral species (A, B and C) obtained by global analysis of the spectral evolution once the steady-state turnover phase has been completed.

and 3-fluorobenzyl alcohols, reflecting formation of the enzyme–substrate complex (Fig. 4B,C) [13,15]. For all substrates, the first spectra produced after mixing quickly evolved to spectral species that remain constant for a while and correspond to the steady-state turnover (lag phase in Fig. 4A). The absorbance of FAD band I during such periods provides information about the flavin redox state during steady-state turnover. The time duration of these lag periods varies with the alcohol substrate, reflecting the relative rates of AAO reduction (by each alcohol) and its oxidation (by O_2) (Fig. 4A). For all the assayed substrates, AAO is predominantly in the oxidized form during this steady-state turnover phase, and the percentage of reduced fraction depends on the alcohol type. For 3-chloro-4-methoxybenzyl, 3-chlorobenzyl and 3-fluorobenzyl alcohols, the AAO oxidized form is highly predominant (95–100%) at the beginning of turnover, indicating that the oxidative half-reaction is much faster than the reductive one. Similar results have previously been observed for 4-methoxybenzyl alcohol (approximately 80% is in the oxidized form) [13]. By contrast, when 3,4-dimethoxybenzyl alcohol was used, the percentage of reduced AAO during turnover increased, up to approximately 40%, indicating that the rates for the reductive and oxidative half-reactions are almost balanced in this case, in agreement with the similar values observed for alcohol and O_2 catalytic efficiencies (Table 1).

The spectral changes after the steady-state turnover phase (the lag phase, Fig. 4A) are indicative of accumulation of reduced AAO (AAO_{red}) as a consequence of decreasing the O_2 concentration in the reaction mixture while alcohol is in excess (Fig. 4). When using 3-chloro-4-methoxybenzyl, 4-methoxybenzyl and 3,4-dimethoxybenzyl alcohols as substrates, such spectral evolution best fitted a two-step process (A → B → C) (Fig. 4B). The first step reflects reduction of the flavin with concomitant formation of a charge transfer complex (CTC) between the reduced enzyme and the aldehyde product of the reaction

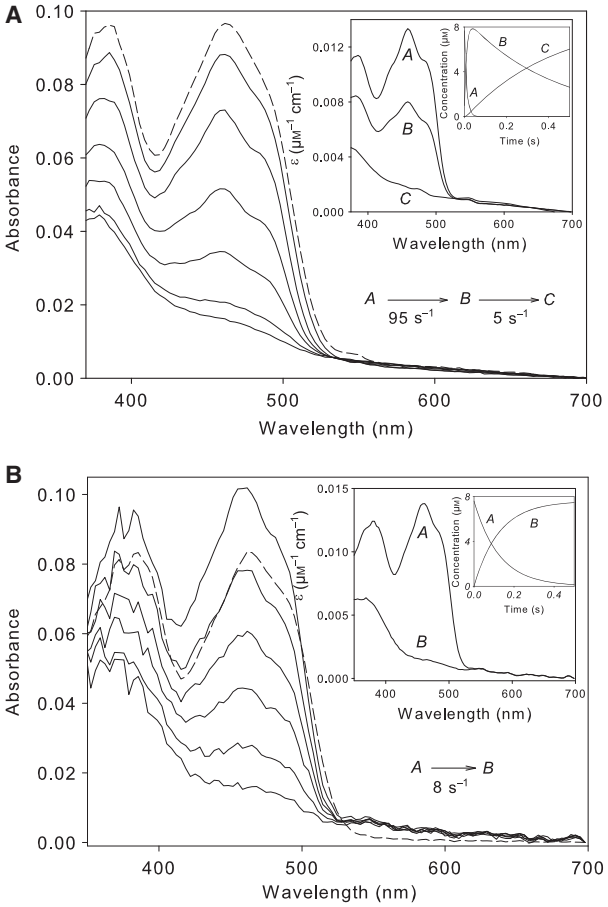

Fig. 5. Pre-steady-state kinetics for the reductive half-reaction of AAO. Spectral time-course of the anaerobic reduction of native AAO (7.5 μM) by 559 μM 3-chloro-4-methoxybenzyl (A) and 2400 μM 3-chlorobenzyl (B) alcohols. The spectrum of the oxidized enzyme before mixing is shown as a dashed line. Spectra after mixing are shown at 4, 19, 39, 80, 330 and 500 ms in (A), and at 2, 39, 78, 129, 219 and 500 ms in (B). The corresponding insets show the absorbance spectra for the two/three kinetically distinguishable spectroscopic species (A, B and C) obtained by global analysis of the spectral evolution. The further insets show the evolution of these species along the reaction course.

previously characterized by a broad band at approximately 550–650 nm [13], and supporting the T-shaped stacking interaction between Tyr92 and the substrate suggested by ligand migration studies (Fig. 1). The second step involves spectral perturbation in the CTC band and the appearance of a new peak at 490 nm. These events (CTC formation and spectral perturbations) may be related to the presence of O_2 in the active site, as the AAO anaerobic reduction by these substrates prevents CTC formation, as described below (Fig. 5). On the other hand, the spectral changes after the steady-state turnover phase when using 3-chlorobenzyl and 3-fluorobenzyl alcohols occurs through a one-step process (A → B), leading directly from oxidized to fully reduced flavin without stabilization of any CTC intermediate (Fig. 4C). These results with various substrates under turnover conditions, together with the steady-state kinetic constants obtained, provide valuable mechanistic information that may be correlated with the pre-steady-state studies as described below.

Stopped-flow spectrophotometry has additionally been used to study the influence of the alcohol type on the AAO reductive half-reaction by monitoring the time course of its reduction under anaerobic conditions in the 350–900 nm range. Under the assayed conditions, the five alcohol substrates fully reduced AAO without production of any FAD semiquinone intermediate (Fig. 5), consistent with a hydride transfer mechanism as reported for 4-methoxybenzyl alcohol and 2,4-hexadien-1-ol [13].

For 3,4-dimethoxybenzyl and 3-chloro-4-methoxybenzyl alcohols, the evolution of spectral changes upon AAO reduction was consistent with a two-step kinetic model (A → B → C) (Fig. 5A), as previously reported for 4-methoxybenzyl alcohol [13]. The first process (A → B) was fast and hyperbolically dependent on substrate concentration, accounting for more than 80% of the reaction amplitude. This step is thought to correspond to substrate oxidation and formation of an AAO_{red}–product complex. The second process (B → C) was concentration-independent and too slow (3–5 s^{-1}) to be relevant for overall turnover (Table 1). This step may be related to a slow release of the aldehyde product from the reduced AAO active site in the absence of O_2 (k_3 in Scheme 1). Formation of such unstable enzyme–product complexes have also been reported in other flavin-dependent oxidases that show a bi-phasic reaction course [29,30]. The hyperbolic dependence of reduction rates (k_{obs}) for the first process was fitted to Eqn (3) or Eqn (4) (see Experimental procedures), consistent with an essentially irreversible flavin reduction (k_{rev} of approximately 0). The calculated reduction constants (k_{red}) for the AAO reduction by 3,4-dimethoxybenzyl and 3-chloro-4-methoxybenzyl alcohols were up to threefold faster than their turnover rates, suggesting that the reductive half-reaction is not the limiting step when these alcohols are oxidized.

For 3-chlorobenzyl and 3-fluorobenzyl alcohols, the first spectra obtained after mixing clearly exhibit displacement and an absorbance increase of the flavin band I. These spectral changes were previously attributed to formation within the dead time of the stopped-flow assay of an initial Michaelis-Menten complex of the oxidized enzyme with the alcohol substrate [15]. The subsequent decrease in absorbance best fitted a

one-step model (A → B), describing an essentially irreversible AAO reduction by 3-chlorobenzyl and 3-fluorobenzyl alcohols (Fig. 5B). The observed rates for this step showed hyperbolic dependence on the substrate concentration, which fitted Eqn (3), indicating that this step includes rearrangements in the initial complex to produce the catalytically competent complex as well as the flavin reduction. The k_{red} values for these two alcohols (8 ± 1 and 6 ± 1 s^{-1}, respectively) were similar to their reported turnover rates (Table 1), clearly indicating that, for these substrates, the reductive half-reaction is the limiting step in catalysis.

Similarly, the AAO oxidative half-reaction was studied by following the flavin absorbance increase at 462 nm after mixing enzyme reduced in advance by incubation with a slight excess of the various alcohol substrates under anaerobiosis with buffer containing known O_2 concentrations. For all reducing substrates, the rates of flavin reoxidation were linearly dependent on O_2 concentration (data not shown), and similar to those reported for other oxidases. The values obtained for second-order rate constants were 7.0×10^5, 8.0×10^5 and 8.4×10^5 $M^{-1} \cdot s^{-1}$ for 3-chlorobenzyl, 3-chloro-4-methoxybenzyl and 3,4-dimethoxybenzyl alcohol, respectively, similar to that previously reported for 4-methoxybenzyl alcohol (6.7×10^5 $M^{-1} \cdot s^{-1}$) [12, 31]. Therefore, the rates of flavin reoxidation are neither dependent on the nature of the alcohol substrate nor on the kinetic mechanism. However, the experimental conditions used do not guarantee the presence of the aldehyde product at the active site during flavin reoxidation.

Stacking stabilization of the substrate in the AAO active site

AAO oxidizes mainly aromatic and other π system-containing conjugated primary alcohols. The aromatic nature of the AAO alcohol substrates suggests the importance of π–π stacking in substrate stabilization by AAO. Ligand migration studies showed a T-shaped interaction between Tyr92 and the alcohol substrate in the catalytically active configurations [18]. Starting from this active complex, the Tyr–substrate binding energy was evaluated using *ab initio* quantum chemistry.

Table 2 shows the T-shaped interaction energies between a tyrosine side chain and five AAO substrates: 4-methoxybenzyl, 3-chloro-4-methoxybenzyl, 3,4-dimethoxybenzyl, 3-chlorobenzyl and 3-fluorobenzyl. For each substrate, we modeled both the alcohol and the aldehyde forms. The first clear result is that all the interaction energies are stabilizing, with similar values to those obtained by others [32]. In all cases, the stabilization energy is slightly higher for the alcohol reactants than for the aldehyde products. This difference facilitates release of the products. Furthermore, important differences were observed for 3-chlorobenzyl and 3-fluorobenzyl alcohols. We observed a lower stacking stabilization for the alcoholic form, and a larger decrease in the interaction energy with the aldehyde. The significantly lower stabilization for the aldehyde product for these two substrates also establishes a direct correlation between lower π–π stacking stabilization energies and the ping–pong mechanism, and the lack of stabilization of any CTC during turnover.

Table 2. T-shaped stacking energies between five AAO alcohol substrates and their corresponding aldehydes with a tyrosine side chain, and differences between the two calculated energies ($kcal \cdot mol^{-1}$).

	Alcohols	Aldehyde	Difference
4-Methoxybenzyl alcohol	−3.27	−2.83	−0.44
3-Chloro-4-methoxybenzyl alcohol	−3.16	−3.00	−0.16
3,4-Dimethoxybenzyl alcohol	−4.11	−3.62	−0.49
3-Chlorobenzyl alcohol	−2.77	−1.96	−0.81
3-Fluorobenzyl alcohol	−2.67	−1.81	−0.86

Kinetic properties for Tyr92 variants

Several site-directed variants of AAO at Tyr92 were prepared to investigate its role in catalysis. The Y92L, Y92F and Y92W variants were purified as oxidized holoproteins, showing an A_{280}/A_{463} ratio of approximately 10, similar to the native enzyme. The absorption spectra of Y92L and Y92F were basically similar to that of the native enzyme, with absorption maxima at 387 and 463 nm, while the maxima for the Y92W variant were slightly displaced at 384 and 457 nm (data not shown).

The catalytic properties of the Y92L, Y92F and Y92W AAO variants were determined using 4-methoxybenzyl alcohol as substrate (Table 3). While mutating the tyrosine to phenylalanine only causes a slight increase in $K_{m(O_2)}$, its replacement with a leucine produces a decrease in catalytic efficiency for the alcohol substrate (2.6-fold lower), accompanied by approximately twofold increases in both $K_{m(Al)}$ and K_d. Finally, the incorporation of a bulkier residue (Y92W mutation) causes a strong decrease in catalytic efficiencies for both O_2 (sixfold lower) and 4-methoxybenzyl alcohol (860-fold lower). As the turnover rate for the Y92W variant was reduced tenfold, we conclude that the main effect of the mutation concerns the availability of the alcohol substrate at the AAO active site (with 75-fold higher K_m values). Likewise, the Y92W mutation prevents CTC formation during enzyme

Table 3. Kinetic parameters for steady-state reaction and for the pre-steady-state reductive half-reaction of native AAO and three Tyr92 variants in the oxidation of 4-methoxybenzyl alcohol.

	Steady-state turnover					Reductive half-reaction	
	k_{cat} (s^{-1})	$K_{m(Al)}$ (μM)	$k_{cat}/K_{m(Al)}$ ($s^{-1}\cdot mM^{-1}$)	$K_{m(Ox)}$ (μM)	$k_{cat}/K_{m(Ox)}$ ($s^{-1}\cdot mM^{-1}$)	k_{red} (s^{-1})	K_d (μM)
AAO[1]	129 ± 5	25 ± 3	5160 ± 650	348 ± 36	371 ± 41	115 ± 3	31 ± 2
Y92F	120 ± 1	30 ± 1	4450 ± 120	147 ± 4	814 ± 21	119 ± 9	42 ± 12
Y92L	100 ± 2	51 ± 2	1940 ± 4	348 ± 13	286 ± 12	95 ± 2	52 ± 4
Y92W	11 ± 0.3	1890 ± 70	6 ± 0.3	181 ± 7	60 ± 3	14 ± 1	4630 ± 520

Measurements were carried out in 0.1 M phosphate buffer, pH 6, at 12 °C. Bisubstrate steady-state constants were determined by varying the concentrations of both alcohol and O_2, and fitting the data to Eqn 1 (native AAO) or Eqn 2 (Y92F, Y92L and Y92W variants) describing ternary and ping-pong mechanisms, respectively (see Materials and Methods). Means and standard deviations are provided. [1]Data from Ferreira *et al.* [13].

turnover with 4-methoxybenzyl alcohol, also suggesting that stacking interactions are strongly affected by this mutation (Fig. 6).

The fast reaction of the tyrosine variants with 4-methoxybenzyl alcohol was also investigated by anaerobic stopped-flow techniques. The spectral evolution obtained for all variants indicated complete (two-electron) enzyme reduction, in agreement with a hydride transfer reaction (Fig. 7). The calculated k_{red} and K_d values agreed with the steady-state k_{cat} and K_m values

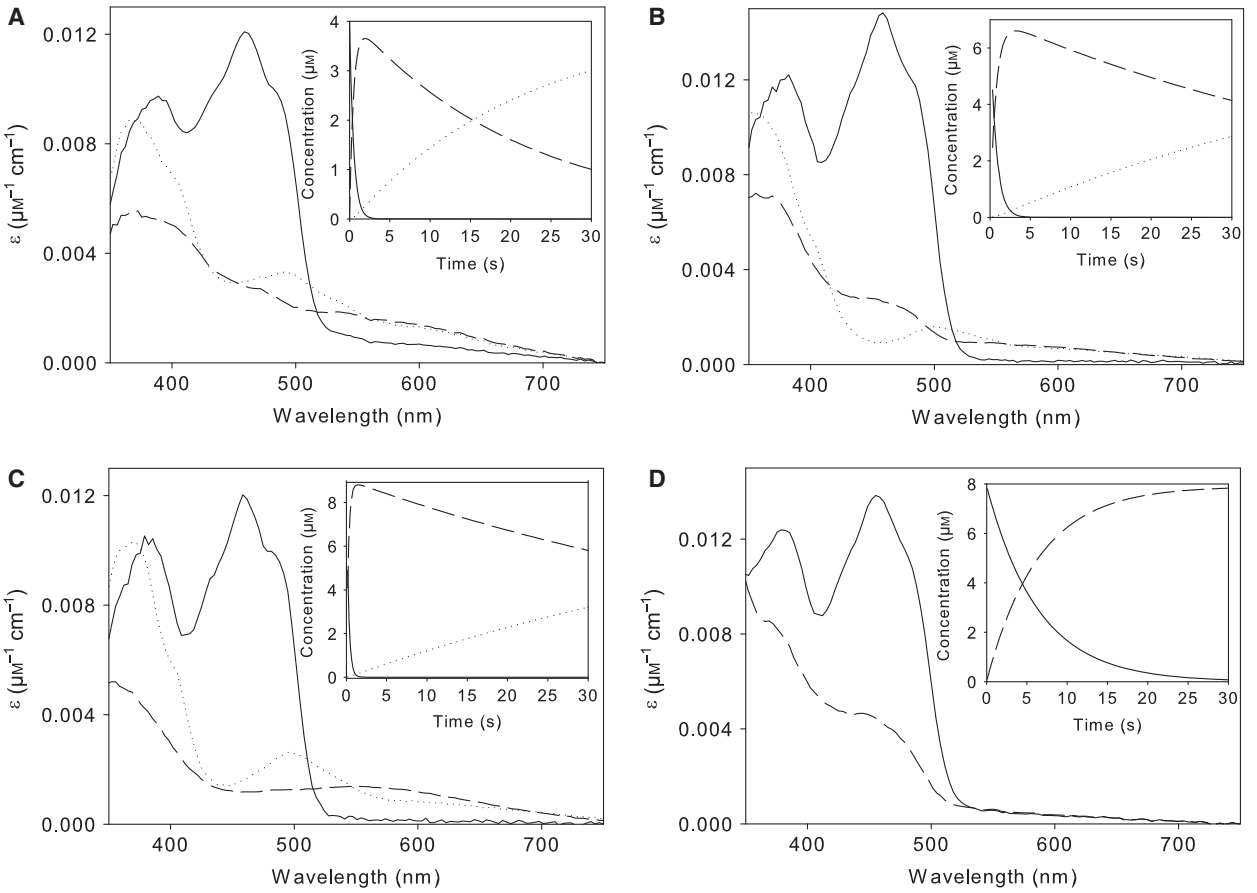

Fig. 6. Spectral species obtained after global analysis of the spectral evolution after the steady-state turnover of native AAO (A) and its Y92L (B), Y92F (C) and Y92W (D) variants. An aerobic solution of AAO (approximately 10 μM, except that for the native protein, which was approximately 5 μM) was reacted in the stopped-flow equipment with saturating concentrations of 4-methoxybenzyl alcohol (1 mM, except that for the Y92W variant, which was 10 mM) in 0.1 M phosphate, pH 6, at 25 °C under aerobic conditions. Species A, B and C are shown as solid, dashed and dotted lines, respectively. The corresponding insets show the evolution of these species along the reaction course.

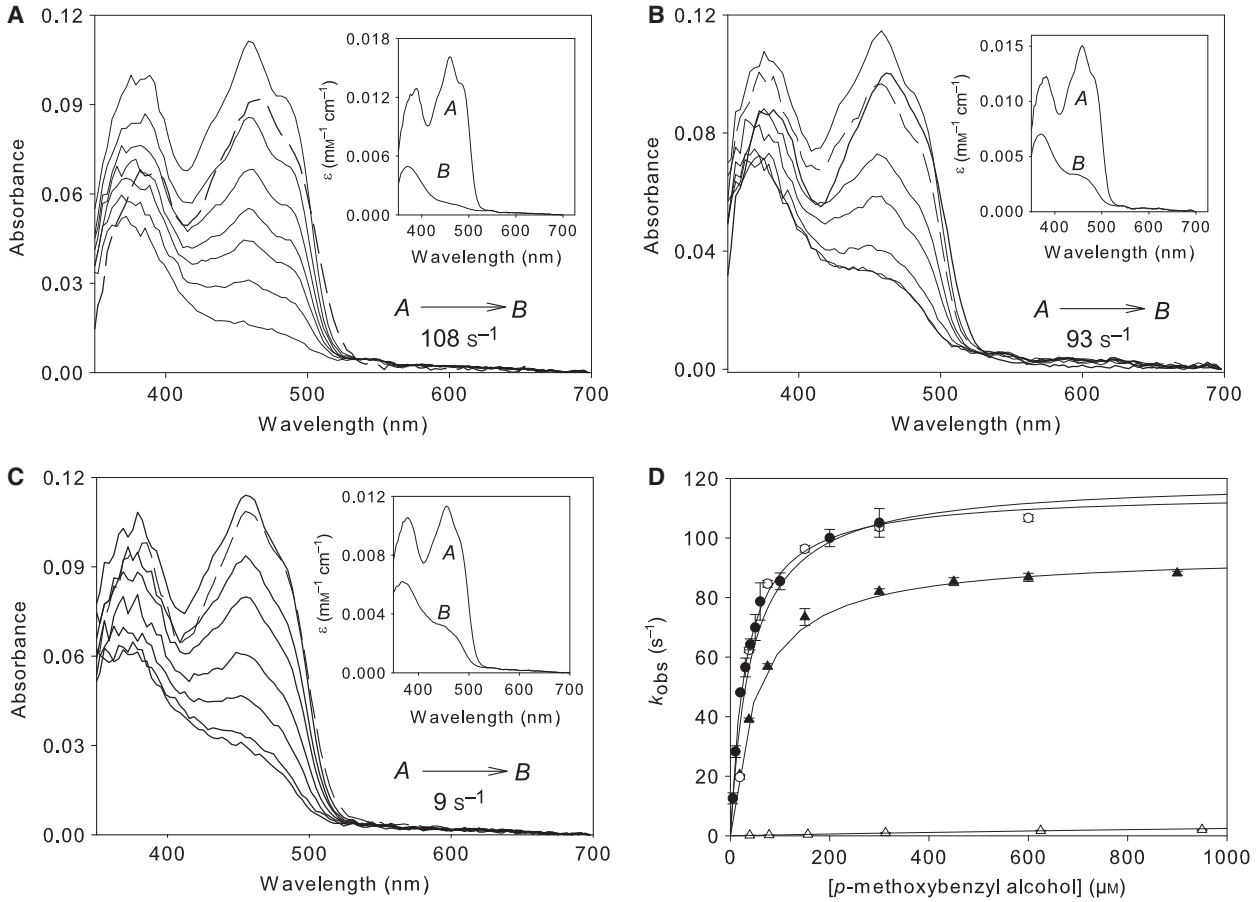

Fig. 7. Pre-steady-state kinetics for the reductive half-reaction of three Tyr92 AAO variants when using 4-methoxybenzyl alcohol as substrate. (A–C) Spectral evolution of the anaerobic reduction of the Y92F (A), Y92L (B) and Y92W (C) AAO variants (9 μM) by 4-methoxybenzyl alcohol. Spectra for the oxidized enzyme before mixing are indicated by dashed lines. Spectra after mixing are shown at 0.004, 0.006, 0.009, 0.0115, 0.0141, 0.0192 and 0.032 s in (A), 0.004, 0.006, 0.012, 0.017, 0.029, 0.099 and 0.25 s in (B), and 0.004, 0.006, 0.03, 0.11, 0.18, 0.44 and 0.98 s in (C). The corresponding insets show the spectra for the kinetically distinguishable species (A and B) obtained by global analysis of the spectral evolution. (D) Dependence of observed rates on the concentrations of 4-methoxybenzyl alcohol by native AAO (black circles) and the Y92F (open circles), Y92L (black triangles) and Y92W (open triangles) AAO variants, fitted to Eqn (5). Assays were performed at 12 °C.

(Table 3), indicating that the reductive half-reaction is the rate-limiting step in catalysis for these variants.

To investigate whether Tyr92, by establishing a stacking interaction with the docked 4-methoxybenzyl alcohol (Fig. 1), contributes to the hydride transfer selectivity previously reported for native AAO [18], we measured the KIEs values for apparent steady-state kinetic constants for the Y92L variant using three isotopically labeled preparations of this alcohol: (*R*)-[α-^{2}H]-, (*S*)-[α-^{2}H]- and [α-^{2}H$_2$]-4-methoxybenzyl alcohol (Table 4). The KIEs on the apparent turnover values, $^{D}(^{app}k_{cat})$, slightly decreased (approximately 20%) for the (*R*) and di-deuterated forms, but were unaffected for the (*S*) form. However, the KIEs on the apparent catalytic efficiency, $^{D}(^{app}k_{cat}/K_{m(Al)})$, for the (*R*) form and especially the di-deuterated alcohols were significantly higher for the Y92L variant, and therefore the $^{D}(K_{m(Al)})$ values were significantly lower than those of the native AAO. In fact, the small $^{D}(K_{m(Al)})$ KIE for native AAO (deuteration mainly affects the $^1H^-/^2H^-$ abstraction ratio) was absent for the Y92L variant (although the KIE on turnover was not modified), indicating that Tyr92 contributes to 4-methoxybenzyl alcohol binding.

Discussion

Ping–pong versus ternary mechanism in AAO and other flavo-oxidases

In comparison with other GMC oxidoreductases, which catalyze the oxidation of alcohol groups in relatively

Table 4. KIEs on apparent steady-state parameters for the oxidation of three α-deuterated *p*-methoxybenzyl alcohols by native AAO and its Y92L variant under O_2 saturation conditions. Steady-state constants were estimated in O_2-saturated (1.279 mM) 0.1 M phosphate, pH 6, at 25 °C. KIEs are the ratio between the activity on protiated and deuterated substrate calculated by fitting constants to Eqn (6). Values are means ± standard deviations. [1]Data for native AAO are from Ferreira *et al.* [13] and Hernandez-Ortega *et al.* [34].

	$^{D}(^{app}k_{cat})$	$^{D}(^{app}K_{m(Al)})$	$^{D}(^{app}k_{cat}/K_{m(Al)})$
Native AAO[1]			
(*R*)-[α-^{2}H]-4-methoxybenzyl alcohol	5.0 ± 0.0	1.3 ± 0.1	3.8 ± 0.1
(*S*)-[α-^{2}H]-4-methoxybenzyl alcohol	1.3 ± 0.0	1.0 ± 0.1	1.3 ± 0.1
[α-$^{2}H_2$]-4-methoxybenzyl alcohol	7.6 ± 0.1	1.9 ± 0.1	4.1 ± 0.1
Y92L variant			
(*R*)-[α-^{2}H]-4-methoxybenzyl alcohol	4.0 ± 0.0	1.0 ± 0.1	4.3. ± 0.1
(*S*)-[α-^{2}H]-4-methoxybenzyl alcohol	1.3 ± 0.0	1.1 ± 0.1	1.2 ± 0.1
[α-$^{2}H_2$]-4-methoxybenzyl alcohol	6.2 ± 0.1	1.1 ± 0.1	5.8 ± 0.1

specific reactions, AAO shows a broad electron donor substrate specificity, oxidizing aromatic and other π system-containing substrates with conjugated primary alcohols (including benzylic, naphthylic and aliphatic polyunsaturated alcohols) [5,14,33]. These *n* systems increase the electron availability at the benzylic position, enabling hydride abstraction by flavin N5. Moreover, the architecture of the AAO active site prevents the oxidation of secondary alcohols that cannot be accommodated at adequate distances from the catalytic histidine and the above-mentioned flavin N5 atom due to the presence of Phe501 [34].

Here we have performed a detailed study on the AAO kinetic mechanism using various alcohol substrates. In all cases, the AAO catalytic reaction may be divided into a reductive half-reaction, in which two electrons are transferred via a hydride ion to the oxidized FAD, and an oxidative half-reaction, in which two electrons are transferred from the reduced flavin to O_2, yielding hydrogen peroxide. However, based on the results of bi-substrate kinetics analysis with various benzylic alcohols, the overall AAO catalytic cycle appears to be highly influenced by the chemical nature of the substituents in the substrate benzenic ring. For electron-withdrawing substituents (in 3-chloro- and 3-fluorobenzyl alcohols), both half-reactions are independent, whereby the aldehyde product dissociation occurs before the O_2 reaction (the second substrate), in a ping–pong steady-state kinetic mechanism (Scheme 1, bottom loop). In contrast, a sequential mechanism operates for alcohols with electron donor substituents (methoxylated benzyl alcohols), in which O_2 reacts with the AAO_{red}–aldehyde complex, forming a ternary complex prior to aldehyde product release (Scheme 1, top loop).

Vanillyl-alcohol oxidase (EC 1.1.3.38), another versatile flavoenzyme that is able to oxidize aromatic alcohols, although belonging to a different superfamily to AAO, also exhibits substrate-dependent overall catalysis [35]. This behavior differs from other fungal GMC oxidoreductases, such as glucose oxidase (EC 1.1.3.4), pyranose 2-oxidase (EC 1.1.3.10), cholesterol oxidase and cellobiose dehydrogenase (EC 1.1.99.18), for which the ping–pong mechamism has been reported as the general mechanism [23,36–38]. Interestingly, detailed investigations on pyranose 2-oxidase recently indicated that its steady-state mechanism alters as a function of pH [39].

Stacking interactions govern AAO catalytic mechanism

Classical force fields semi-quantitatively reproduce T-shaped stacking dispersion forces [40]. Moreover, high-level QM studies have indicated the importance of T-shaped interactions in molecular stacking, for example in benzene dimers [41]. In AAO, previous ligand migration simulations (using classical force fields) [18] suggested a T-shaped substrate–Tyr92 interaction. Our QM calculations (Table 2) confirm such stabilizing interactions for the various substrate (alcohol)/product (aldehyde) benzenic rings. In addition, stacking energies estimated for the various substrates/products correlate fairly well with the electron-donating/withdrawing properties (to the ring π cloud) of their various substituents. The nucleophilicity of methoxybenzene is stronger than that of benzene due to resonance, increasing the electronic density in the ring. These effects explain why dimethoxylated alcohols/aldehydes have the largest stacking interaction energies. On the other hand, for 3-chloro- and 3-fluoro-substituted alcohols/aldehydes, the halogen acts as an electron withdrawer (inductive effect), resulting in the lowest stabilization energies. Moreover, the slightly different interaction energies for these two halogenated compounds follow the expected trend for the increased electronegativity of the fluoride compared to chloride, and thus stronger inductive electron-withdrawing effects. Thus, the lower interaction energies for the two halogenated aldehydes compared with the methoxylated aldehydes, together with the higher alcohol–aldehyde differential interaction energies, contribute to release of the aldehyde product, favoring the

ping–pong mechanism. The stacking interactions were intermediate for the 3-chloro-4-methoxybenzyl alcohol/aldehyde due to the combination of electron donor and withdrawing substituents.

Taking together the kinetic data, the stacking energy calculations and the available structural and computational information reported previously, the overall AAO catalytic cycle is consistent with the proposed kinetic model of Scheme 1. Substrate diffusion studies showed that alcohol and O_2 molecules access the AAO active site through the same hydrophobic channel [12,18]. However, the alcohol diffusion pathway requires chain displacements and interaction with residues Phe397, Tyr92 and Phe501 to reach the AAO active site, while O_2 diffusion does not require any rearrangement. This continuous O_2 supply supports the finding that, for the sequential mechanism, where the aldehyde product is still bound at the active site when O_2 reaches it, some arrangement of the aldehyde product for flavin reoxidation is required (for more detail, see Movie S1 in [12,18]). However, the O_2 affinity increases when the reaction occurs with alcohols, leading to a ping–pong mechanism. This may be caused by prior dissociation of product aldehyde, leaving more space at the active site for O_2 binding.

Rate-limiting step(s) in AAO catalysis

Rapid kinetic experiments provided information on the reductive and oxidative half-reactions for each alcohol substrate. For the 3-chlorobenzyl and 3-fluorobenzyl alcohols, the reductive half-reaction is the rate-determining step in catalysis, and is responsible of the low efficiency of substrate oxidation.

However, for 3,4-dimethoxybenzyl and 3-chloro-4-methoxybenzyl alcohols, the flavin reduction rate is far from being the limiting state. In the first case, the apparent second-order constant estimated from pre-steady kinetic data (k_{red}/K_d = 156 ± 46 $s^{-1}\cdot mM^{-1}$) is in agreement with the steady-state alcohol catalytic efficiency obtained (105 ± 8 $s^{-1}\cdot mM^{-1}$). In the ternary complex mechanism shown in Scheme 1 (top loop), k_{cat} is a combination of catalytic steps in which the 3,4-dimethoxybenzyl alcohol is oxidized to 3,4-dimethoxybenzaldehyde (k_2 approximately equal to k_{red}) and the product is released (k_5) [$k_{cat} = k_2\ k_5/(k_2 + k_5)$]. The estimated value for k_5 (101 s^{-1}) is indicative of a partially rate-limiting step for catalysis, suggesting that another kinetic step (after hydride transfer and before product release) also contributes to limiting the reaction rate. This step may be atributted to the flavin reoxidation, as suggested by the fact that 40% of AAO is reduced during enzyme turnover with this substrate showing similar catalytic efficiencies for alcohol and O_2. Finally, for 3-chloro-4-methoxybenzyl alcohol oxidation, the estimated k_5 value (42 s^{-1}) suggests that product release may be the rate-limiting step (Scheme 1, top loop). In fact, previous studies on 3-chloro-4-methoxybenzyl alcohol oxidation by AAO indicate that a proportion of the aldehyde formed was oxidized to the corresponding acid, rather than being released from the active site [15].

Regarding the oxidative half-reaction, reoxidation of AAO, previously reduced by different alcohols, yielded bi-molecular rate constants ($7.0 \times 10^5 - 8.4 \times 10^5$ $M^{-1}\cdot s^{-1}$) in the range typical of other flavo-oxidases, and approximately three orders of magnitude larger that the values reported for non-enzymatic reoxidation of free flavins (250 $M^{-1}\cdot s^{-1}$) [31,42]. This is consistent with enhanced O_2 reactivity of AAO when the conserved active site His502 is protonated during the oxidative half-reaction, reducing the singlet/triplet energy gap [10]. The importance of a positively charged group for O_2 activation has been reported for flavoprotein oxidases [31,43].

Role of Tyr92 in AAO catalysis

Finally, the kinetic data obtained here for the Tyr92 variants strongly suggest that this residue is involved in alcohol substrate stabilization at the AAO active site. The Y92F variant exhibits similar rates for 3-methoxybenzyl alcohol oxidation to the native enzyme, while the leucine and tryptophan substitutions mainly alter the alcohol substrate affinity. In the case of the Y92W variant, the substrate binding significantly weakened, with 76- and 150-fold higher K_m and K_d values, respectively. However, changes to the affinity constants for the Y92L variant were modest, suggesting that some stacking is still possible. In fact, the Y92L and Y92F mutants are capable of forming CTC, indicating that both proteins stabilize stacking interactions. In a previous study, Tyr92 substitution with alanine (fully removing the stacking interaction) did not yield active enzyme, supporting involvement of the above-mentioned π–π interaction in AAO catalysis [17]. Interestingly, Tyr92 is not conserved in the GMC oxidoreductase superfamily. However, tyrosine, phenylalanine and leucine residues are frequently found at this position in the putative AAO sequences from various basidiomycetes genomes (Fig. 8). This suggests that stacking may be a common catalytic strategy for alcohol substrate oxidation in AAO enzymes.

In conclusion, the study of the overall catalytic cycle of AAO presented here shows that the stacking-stabilizing interaction of the aromatic substrate/product by

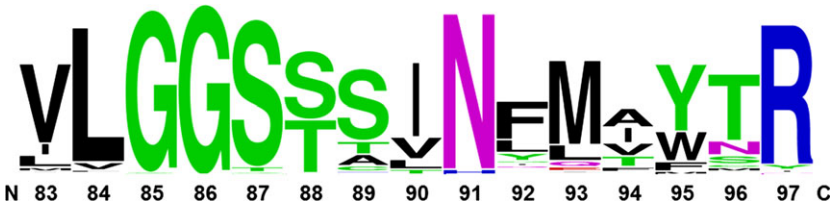

Fig. 8. Sequence logo for 70 putative AAO sequences from various basidiomycetes corresponding to positions 83–97 of mature *P. eryngii* AAO generated using WebLogo [51]. The compared sequences were taken from the following genomes available at the Joint Genome Institute (www.jgi.doe.gov); the numbers of AAO sequences are indicated in parentheses: *Bjerkandera adusta* (11), *Dichomitus squalens* (9), *Fomitiporia mediterranea* (1), *Fomitopsis pinicola* (1), *Ganoderma* sp. (7), *Gelatoporia subvermispora* (4), *Gloeophyllum trabeum* (2), *Laccaria bicolor* (1), *Phanerochaete chrysosporium* (3), *Phlebia brevispora* (3), *Punctularia strigosozonata* (6), *Rhodonia placenta* (2), *Stereum hirsutum* (15) and *Trametes versicolor* (3). The numbers indicate the position in the mature *P. eryngii* AAO sequence, the overall height of each letter reflects the sequence conservation at that position, and the heights of symbols in the same column indicate the relative frequency of each amino acid.

active-site Tyr92 governs AAO catalysis, switching between the ping–pong and the ternary mechanism depending on the stacking stabilization energies. The importance of Tyr92 for alcohol substrate binding was also demonstrated by site-directed mutagenesis, kinetics and KIE studies, suggesting a common role in other AAO proteins where this residue is conserved or replaced by others that are able to establish similar stacking interactions.

Experimental procedures

Chemicals

4-methoxybenzyl, 3,4-dimethoxybenzyl (veratryl), 3-chlorobenzyl and 3-fluorobenzyl alcohols were purchased from Sigma-Aldrich (St Louis, MO, USA). 3-chloro-4-methoxybenzyl alcohol, (*R*)-[α-^{2}H]-4-methoxybenzyl alcohol, (*S*)-[α-^{2}H]-4-methoxybenzyl alcohol and [α-$^{2}H_2$]-4-methoxybenzyl alcohol were synthesized at the Instituto de Ciencia de Materiales de Aragón (Zaragoza, Spain).

Protein production and purification

Native AAO from *P. eryngii* was obtained by expression in *Escherichia coli* of the mature AAO cDNA (GenBank accession number AF064069), followed by *in vitro* activation in the presence of the FAD cofactor, and purification by ion-exchange chromatography as described previously [44]. Mutated variants were prepared using a QuikChange site-directed mutagenesis kit (Stratagene, Santa Clara, CA, USA). For the PCR reactions, cDNA cloned into the pFLAG1 vector was used as the template, and the following oligonucleotides (direct sequences) bearing mutations (shown in bold italics) as primers: (a) Y92L, 5′-GGGTCTAGCTCTGTTCAC***CT***CATGGTCATGATGCG-3′, (b) Y92F, 5′-GGGTCTAGCTCTGTTCACT***T***CATGGTCATGATGCG-3′, and (c) Y92W, 5′-GGGTCTAGCTCTGTTCACT***GG***ATGGTCATGATGCG-3′ [44]. Mutations were confirmed by sequencing using a GS-FLX sequencer (Roche, Basel, Switzerland), and the mutated variants were obtained as described for recombinant AAO. The naturally oxidized AAO concentration was determined using the molar absorbances of native AAO and of its Y92L, Y92F and Y92W variants (ε_{463} = 11 050 $M^{-1}\cdot cm^{-1}$, ε_{463} = 11 240 $M^{-1}\cdot cm^{-1}$, ε_{463} = 10 044 $M^{-1}\cdot cm^{-1}$ and ε_{457} = 10 693 $M^{-1}\cdot cm^{-1}$, respectively) calculated by heat denaturation and estimation of the free FAD released (ε_{450} 11 300 $M^{-1}\cdot cm^{-1}$) [44].

Steady-state kinetic measurements

Steady-state kinetics data were spectrophotometrically obtained by following the oxidation of the alcohol substrate to the corresponding aldehyde as previously described [14]. Two-substrate steady-state kinetics measurements were performed by simultaneously varying the concentrations of O_2 and alcohol substrate in 0.1 M phosphate buffer, pH 6, at 12 °C. Due to large differences in AAO affinities for these alcohols, the concentrations were in the ranges of 8.7–279, 31.3–4000, 7.8–2000 and 39–4000 μM for 3-chloro-4-methoxybenzyl, 3,4-dimethoxybenzyl, 3-chlorobenzyl and 3-fluorobenzyl alcohols, respectively. The reactions were performed in a screw-cap cuvette in which the buffer solution was first equilibrated at the desired concentration of O_2 (61, 152, 319, 668 and 1520 μM at 12 °C) by bubbling with the appropriate O_2/N_2 gas mixture for 10–15 min. Then, reactions were started by addition of the alcohol substrate (approximately 5–10 μL) and AAO (5 μL, 0.03 μM final concentration) into a reaction mixture with a final volume of 1.5 mL. Initial rates were calculated during the linear phase of alcohol oxidation to the corresponding aldehyde, and analyzed by fitting to Eqn (1) or Eqn (2), describing ternary complex and ping–pong mechanisms, respectively:

$$\frac{v}{e} = \frac{k_{cat}AB}{K_{m(Ox)}A + K_{m(Al)}B + AB + K_{i(Al)}K_{m(Ox)}} \quad (1)$$

$$\frac{v}{e} = \frac{k_{cat}AB}{K_{m(Ox)}A + K_{m(Al)}B + AB} \quad (2)$$

where v represents the observed initial rate, e is the enzyme concentration, k_{cat} is the maximal turnover, A is the alcohol substrate concentration, B is the O_2 concentration, $K_{m(Al)}$ and $K_{m(Ox)}$ are the Michaelis-Menten constants for alcohol and O_2, respectively, and $K_{i(Al)}$ is the alcohol dissociation constant.

Stopped-flow measurements: enzyme turnover and pre-steady-state kinetics

Stopped-flow experiments were performed on an Applied Photophysics SX17.MV spectrophotometer using SX18.MV or XSCAN software for experiments with single wavelength or photodiode-array detection, respectively (Applied Photophysics, Leatherhead, Surrey, UK). For enzyme-monitored turnover experiments, air-saturated enzyme and substrate solutions were mixed, and the evolution of the flavin redox state was monitored in the range 350–900 nm.

Reductive half-reaction studies were performed under anaerobic conditions. Tonometers containing enzyme and substrate solutions were made anaerobic by successive evacuation and flushing with argon. These solutions also contained glucose (10 mM) and glucose oxidase (10 $U \cdot mL^{-1}$) to ensure anaerobiosis. Drive syringes in the stopped-flow apparatus were made anaerobic by sequential passing through of a sodium dithionite solution and O_2-free buffer [45]. The substrate concentrations used were in the range 0.195–12.5, 0.035–0.559, 0.037–2.4 and 0.039–9.9 mM for 3,4-dimethoxybenzyl, 3-chloro-4-methoxybenzyl, 3-chlorobenzyl and 3-fluorobenzyl alcohols, respectively. Measurements were performed in 0.1 M phosphate buffer, pH 6, at 12 °C. All given concentrations are those after mixing an equal volume of substrate and enzyme (i.e. final concentrations). Spectral evolution was studied by global analysis and numerical integration methods using PRO-K software (Applied Photophysics). Observed rate constants (k_{obs}) from traces recorded at 462 nm were calculated from exponential fits. Rate constants were obtained by non-linear fitting of k_{obs} at various substrate concentrations to either Eqn (3) or Eqn (4):

$$k_{obs} = \frac{k_{red}A}{K_d + A} \quad (3)$$

$$k_{obs} = \frac{k_{red}A}{K_d + A} + k_{rev} \quad (4)$$

where k_{obs} is the observed rate for reduction of the enzyme at a given alcohol concentration, k_{red} and k_{rev} are the limiting rates for hydride transfer from the substrate to the flavin and for the reverse reaction, respectively, at saturating substrate concentrations, and K_d is the dissociation constant for the enzyme–substrate complex.

Rate constants for the oxidative half-reaction were measured at 12 °C in 0.1 M phosphate buffer by monitoring the absorbance increase at 462 nm upon mixing the previously anaerobically reduced enzyme with buffer equilibrated at various O_2 concentrations. The enzyme was reduced either by mixing the oxidized protein under anaerobic conditions with a 1.2-fold excess of the corresponding alcohol substrate or by photoreduction in the presence of 2 mM 5-deazariboflavin and 3 mM EDTA [14]. The apparent second-order rate constants for the oxidative half-reaction (k_{ox}) were determined as a function of the O_2 concentrations, and calculated using Eqn (5), where the k_{obs} is the experimentally observed rate constant associated with flavin oxidation at any given O_2 concentration:

$$k_{obs} = {}^{app}k_{ox}[O_2] \quad (5)$$

KIEs for *p*-methoxybenzyl alcohol oxidation

The substrate KIEs on apparent steady-state kinetic constants due to *p*-methoxybenzyl alcohol α-deuteration (*R*, *S* and di-deuterated forms) were measured in O_2-saturated (1.279 mM) 0.1 M phosphate buffer, pH 6.0 at 25 °C. The substrate KIEs were calculated by fitting the initial rates to Eqn (6), which describes a mechanism with separate isotope effects on k_{cat} and k_{cat}/K_m:

$$\frac{v}{e} = \frac{k_{cat}S}{K_m(1 + F_i E_{\frac{k_{cat}}{K_m}}) + S(1 + F_i E_{k_{cat}})} \quad (6)$$

where S is the substrate concentration, F_i is the atom fraction of deuterium label in the substrate (0.98 in the present case), and E_{k_{cat}/K_m} and $E_{k_{cat}}$ are the isotope effect minus 1 on the two kinetic constants [46].

QM calculations

Second-order Moller–Plesset (MP2) [47] QM calculations were performed using the Gaussian03 program (Gaussian Inc., Wallingford, CT, 2004). Triple-zeta split-valence basis sets with polarization orbitals (6-311G*) were used throughout. The structures of the T-shaped complexes between a model tyrosine side chain and the 4-methoxybenzyl alcohol were optimized using MP2 in gas phase, and the most stable structure was selected. To isolate the stacking interactions and avoid distortions from the gas-phase minimization for the remaining complexes, the H atom in the *meta* position of the methoxybenzyl structure was replaced by a chloride or a methoxy group. The 3-chlorobenzyl alco-

hol was obtained by removing the *para* methoxyl from the 3-chloro-4-methoxybenzyl, while the 3-fluorobenzyl alcohol structure was obtained by a chloride to fluoride change in 3-chlorobenzyl alcohol. At this point, the benzene rings are maintained frozen and all substituents are optimized. This procedure was performed for both the alcohol and aldehyde forms. Binding energies were approximated from the interaction energies: AB – (A + B) (where AB stands for the tyrosine-substrate complex) for all complexes, and basis-set superposition error (BSSE) corrections [48] were included at the same level of theory. Several studies on substituted benzene dimers have shown that this level of theory is capable of a qualitative description of differences in stabilization energies [49].

Acknowledgements

This work was supported by grants from the Spanish Ministry of Economy and Competitiveness (MINECO) [grant number BIO2013-42978-P (to M.M.), grant number BIO2011-26694 (to A.T.M.), a 'Juan de la Cierva' sub-program grant (to F.L.) and grant number CTQ2010-18123 (to V.G.)] and by European projects INDOX (grant number KBBE-2013-7-613549, to A.T.M.) and PELE (grant number ERC-2009-Adg 25027, to V.G.).

Author contributions

All of the authors performed the research and discussed the results obtained. P.F. conceived the study, performed some kinetics studies, produced the figures, and wrote the paper, A.H.-O. designed and constructed the mutants, and performed some kinetic studies. F.L., K.W.B. and V.G. performed the computational part of the work, and wrote the corresponding sections of the paper. J.C. produced and characterized the protein variants and produced the figures. B.H. performed some kinetic studies. A.T.M. and M.M. integrated the results and wrote the paper.

References

1 Hernandez-Ortega A, Ferreira P & Martinez AT (2012) Fungal aryl-alcohol oxidase: a peroxide-producing flavoenzyme involved in lignin degradation. *Appl Microbiol Biotechnol* **93**, 1395–1410.
2 Farmer VC, Henderson ME & Russell JD (1960) Aromatic-alcohol-oxidase activity in the growth medium of *Polystictus versicolor*. *Biochem J* **74**, 257–262.
3 Bourbonnais R & Paice MG (1988) Veratryl alcohol oxidases from the lignin-degrading basidiomycete *Pleurotus sajor-caju*. *Biochem J* **255**, 445–450.
4 Sannia G, Limongi P, Cocca E, Buonocore F, Nitti G & Giardina P (1991) Purification and characterization of a veratryl alcohol oxidase enzyme from the lignin degrading basidiomycete *Pleurotus ostreatus*. *Biochim Biophys Acta* **1073**, 114–119.
5 Guillen F, Martinez AT & Martinez MJ (1992) Substrate specificity and properties of the aryl-alcohol oxidase from the ligninolytic fungus *Pleurotus eryngii*. *Eur J Biochem* **209**, 603–611.
6 Asada Y, Watanabe A, Ohtsu Y & Kuwahara M (1995) Purification and characterization of an aryl-alcohol oxidase from the lignin-degrading basidiomycete *Phanerochaete chrysosporium*. *Biosci Biotechnol Biochem* **59**, 1339–1341.
7 Muheim A, Waldner R, Leisola MSA & Fiechter A (1990) An extracellular aryl-alcohol oxidase from the white-rot fungus *Bjerkandera adusta*. *Enzyme Microb Technol* **12**, 204–209.
8 Ruiz-Duenas FJ & Martinez AT (2009) Microbial degradation of lignin: how a bulky recalcitrant polymer is efficiently recycled in nature and how we can take advantage of this. *Microb Biotechnol* **2**, 164–177.
9 Martinez AT, Speranza M, Ruiz-Duenas FJ, Ferreira P, Camarero S, Guillen F, Martinez MJ, Gutierrez A & del Rio JC (2005) Biodegradation of lignocellulosics: microbial, chemical, and enzymatic aspects of the fungal attack of lignin. *Int Microbiol* **8**, 195–204.
10 Hernandez-Ortega A, Lucas F, Ferreira P, Medina M, Guallar V & Martinez AT (2012) Role of active site histidines in the two half-reactions of the aryl-alcohol oxidase catalytic cycle. *Biochemistry* **51**, 6595–6608.
11 Hernandez-Ortega A, Ferreira P, Merino P, Medina M, Guallar V & Martinez AT. Stereoselective hydride transfer by aryl-alcohol oxidase, a member of the GMC superfamily. *ChemBioChem* **13**, 427–435.
12 Hernandez-Ortega A, Lucas F, Ferreira P, Medina M, Guallar V & Martinez AT (2011) Modulating O2 reactivity in a fungal flavoenzyme: involvement of aryl-alcohol oxidase Phe-501 contiguous to catalytic histidine. *J Biol Chem* **286**, 41105–41114.
13 Ferreira P, Hernandez-Ortega A, Herguedas B, Martinez AT & Medina M (2009) Aryl-alcohol oxidase involved in lignin degradation: a mechanistic study based on steady and pre-steady state kinetics and primary and solvent isotope effects with two alcohol substrates. *J Biol Chem* **284**, 24840–24847.
14 Ferreira P, Medina M, Guillen F, Martinez MJ, Van Berkel WJ & Martinez AT (2005) Spectral and catalytic properties of aryl-alcohol oxidase, a fungal flavoenzyme acting on polyunsaturated alcohols. *Biochem J* **389**, 731–738.
15 Ferreira P, Hernandez-Ortega A, Herguedas B, Rencoret J, Gutierrez A, Martinez MJ, Jimenez-Barbero J, Medina M & Martinez AT (2009) Kinetic

and chemical characterization of aldehyde oxidation by fungal aryl-alcohol oxidase. *Biochem J* **425**, 585–593.
16 Fernandez IS, Ruiz-Duenas FJ, Santillana E, Ferreira P, Martinez MJ, Martinez AT & Romero A (2009) Novel structural features in the GMC family of oxidoreductases revealed by the crystal structure of fungal aryl-alcohol oxidase. *Acta Crystallogr D Biol Crystallogr* **65**, 1196–1205.
17 Ferreira P, Ruiz-Duenas FJ, Martinez MJ, van Berkel WJ & Martinez AT (2006) Site-directed mutagenesis of selected residues at the active site of aryl-alcohol oxidase, an H2O2-producing ligninolytic enzyme. *FEBS J* **273**, 4878–4888.
18 Hernandez-Ortega A, Borrelli K, Ferreira P, Medina M, Martinez AT & Guallar V (2011) Substrate diffusion and oxidation in GMC oxidoreductases: an experimental and computational study on fungal aryl-alcohol oxidase. *Biochem J* **436**, 341–350.
19 Hecht HJ, Kalisz HM, Hendle J, Schmid RD & Schomburg D (1993) Crystal-structure of glucose-oxidase from *Aspergillus niger* refined at 2.3 angstrom resolution. *J Mol Biol* **229**, 153–172.
20 Yue QK, Kass IJ, Sampson NS & Vrielink A (1999) Crystal structure determination of cholesterol oxidase from Streptomyces and structural characterization of key active site mutants. *Biochemistry* **38**, 4277–4286.
21 Lario PI, Sampson N & Vrielink A (2003) Sub-atomic resolution crystal structure of cholesterol oxidase: what atomic resolution crystallography reveals about enzyme mechanism and the role of the FAD cofactor in redox activity. *J Mol Biol* **326**, 1635–1650.
22 Kass IJ & Sampson NS (1998) Evaluation of the role of His447 in the reaction catalyzed by cholesterol oxidase. *Biochemistry* **37**, 17990–18000.
23 Hallberg BM, Henriksson G, Pettersson G, Vasella A & Divne C (2003) Mechanism of the reductive half-reaction in cellobiose dehydrogenase. *J Biol Chem* **278**, 7160–7166.
24 Hallberg BM, Henriksson G, Pettersson G & Divne C (2002) Crystal structure of the flavoprotein domain of the extracellular flavocytochrome cellobiose dehydrogenase. *J Mol Biol* **315**, 421–434.
25 Kass IJ & Sampson NS (1998) The importance of GLU361 position in the reaction catalyzed by cholesterol oxidase. *Bioorg Med Chem Lett* **8**, 2663–2668.
26 Menon V, Hsieh CT & Fitzpatrick PF (1995) Substituted alcohols as mechanistic probes of alcohol oxidase. *Bioorg Chem* **23**, 42–53.
27 Fan F & Gadda G (2005) On the catalytic mechanism of choline oxidase. *J Am Chem Soc* **127**, 2067–2074.
28 Carro J, Ferreira P, Rodríguez L, Prieto A, Serrano A, Balcells B, Arda A, Jiménez-Barbero J, Gutiérrez A, Ullrich R *et al.* (2014) 5-Hydroxymethylfurfural conversion by fungal aryl-alcohol oxidase and unspecific peroxygenase. *FEBS J.* doi: 10.1111/febs.13177.
29 Pollegioni L, Wels G, Pilone MS & Ghisla S (1999) Kinetic mechanisms of cholesterol oxidase from *Streptomyces hygroscopicus* and *Brevibacterium sterolicum*. *Eur J Biochem* **264**, 140–151.
30 Prongjit M, Sucharitakul J, Wongnate T, Haltrich D & Chaiyen P (2009) Kinetic mechanism of pyranose 2-oxidase from *Trametes multicolor*. *Biochemistry* **48**, 4170–4180.
31 Mattevi A (2006) To be or not to be an oxidase: challenging the oxygen reactivity of flavoenzymes. *Trends Biochem Sci* **31**, 276–283.
32 Mutasem OS & Sherrill DC (2003) Unexpected substituent effects in face-to-face π-stacking interactions. *J Phys Chem* **107**, 8377–8379.
33 Romero E, Ferreira P, Martinez AT & Martinez MJ (2009) New oxidase from Bjerkandera arthroconidial anamorph that oxidizes both phenolic and nonphenolic benzyl alcohols. *Biochim Biophys Acta* **1794**, 689–697.
34 Hernandez-Ortega A, Ferreira P, Merino P, Medina M, Guallar V & Martinez AT (2012) Stereoselective hydride transfer by aryl-alcohol oxidase, a member of the GMC superfamily. *ChemBioChem* **13**, 427–435.
35 Fraaije MW & van Berkel WJ (1997) Catalytic mechanism of the oxidative demethylation of 4-(methoxymethyl)phenol by vanillyl-alcohol oxidase. Evidence for formation of a p-quinone methide intermediate. *J Biol Chem* **272**, 18111–18116.
36 Gibson QH, Swoboda BE & Massey V (1964) Kinetics and mechanism of action of glucose oxidase. *J Biol Chem* **239**, 3927–3934.
37 Artolozaga MJ, Kubatova E, Volc J & Kalisz HM (1997) Pyranose 2-oxidase from *Phanerochaete chrysosporium* further biochemical characterisation. *Appl Microbiol Biotechnol* **47**, 508–514.
38 Kujawa M, Ebner H, Leitner C, Hallberg BM, Prongjit M, Sucharitakul J, Ludwig R, Rudsander U, Peterbauer C, Chaiyen P *et al.* (2006) Structural basis for substrate binding and regioselective oxidation of monosaccharides at C3 by pyranose 2-oxidase. *J Biol Chem* **281**, 35104–35115.
39 Rungsrisuriyachai K & Gadda G (2009) A pH switch affects the steady-state kinetic mechanism of pyranose 2-oxidase from *Trametes ochracea*. *Arch Biochem Biophys* **483**, 10–15.
40 Sherrill CD, Takatani T & Hohenstein EG (2009) An assessment of theoretical methods for nonbonded interactions: comparison to complete basis set limit coupled-cluster potential energy curves for the benzene dimer, the methane dimer, benzene-methane, and benzene-H2S. *J Phys Chem A* **113**, 10146–10159.
41 Dinadayalane TC & Leszczynski J (2009) Geometries and stabilities of various configurations of benzene

dimer: details of novel V-shaped structure revealed. *Struct Chem* **20**, 11–20.
42 Massey V (1994) Activation of molecular oxygen by flavins and flavoproteins. *J Biol Chem* **269**, 22459–22462.
43 Gadda G (2012) Oxygen activation in flavoprotein oxidases: the importance of being positive. *Biochemistry* **51**, 2662–2669.
44 Ruiz-Duenas FJ, Ferreira P, Martinez MJ & Martinez AT (2006) *In vitro* activation, purification, and characterization of Escherichia coli expressed aryl-alcohol oxidase, a unique H2O2-producing enzyme. *Protein Expr Purif* **45**, 191–199.
45 Medina M, Martinez-Julvez M, Hurley JK, Tollin G & Gomez-Moreno C (1998) Involvement of glutamic acid 301 in the catalytic mechanism of ferredoxin-NADP+ reductase from Anabaena PCC 7119. *Biochemistry* **37**, 2715–2728.
46 Sobrado P, Daubner SC & Fitzpatrick PF (2001) Probing the relative timing of hydrogen abstraction steps in the flavocytochrome b2 reaction with primary and solvent deuterium isotope effects and mutant enzymes. *Biochemistry* **40**, 994–1001.
47 Wilson AK, Woon DE, Peterson KA & Dunning TH (1999) Gaussian basis sets for use in correlated molecular calculations. IX. The atoms gallium through krypton. *J Phys Chem* **110**, 7667–7676.
48 Boys SF & Bernardi F (1970) The calculation of small molecular interactions by the differences of separate total energies. Some procedures with reduced errors. *Mol Phys* **19**, 553–566.
49 Lee EC, Kim D, Jurecka P, Tarakeshwar P, Hobza P & Kim KS (2007) Understanding of assembly phenomena by aromatic-aromatic interactions: benzene dimer and the substituted systems. *J Phys Chem A* **111**, 3446–3457.
50 Borrelli KW, Cossins B & Guallar V (2010) Exploring hierarchical refinement techniques for induced fit docking with protein and ligand flexibility. *J Comput Chem* **31**, 1224–1235.
51 Crooks GE, Hon G, Chandonia JM & Brenner SE (2004) WebLogo: A sequence logo generator. *Genome Res* **14**, 1188–1190.